Advances in Materials
2025, Vol. 14, No. 4, pp. 95-104
https://doi.org/10.11648/j.am.20251405.12

Research Article

Investigation on Buffer Layers Influence on the Internal Quantum Efficiency of $CH_3NH_3Sn_{(1-y)}Ge_yI_3$ Lead-Free Perovskite-Based Solar Cells

Saliou Seck*, Alioune Sow, Mamadou Salif Mane, Modou Faye, El Hadji Mamadou Keita, Amadou Ndiaye, Bachirou Ndiaye, Babacar Mbow, Cheikh Sene

Department of Physics, Cheikh Anta Diop University, Dakar, Senegal

Abstract

In this work, we have carried out a study in the modeling of photovoltaic devices based on lead-free perovskite materials, such as $CH_3NH_3Sn_{(1-y)}Ge_yI_3$, in which the germanium content varies from 0 to 1, using thin ZnO, TiO_2 or SnO_2, films as window layers. Thin Cu_2O or NiO layers used as buffer layers ensure the n-p junction with the perovskite absorber material and act as an interface layer with the transport window layer. With the above window and buffer layer materials, photovoltaic devices have been designed. The study highlights the influence of geometric parameters such as the diffusion length of the minority carriers in the buffer layer as well as the thickness of this layer on the performance of photovoltaic devices. The evolution of the internal quantum efficiency is analyzed as a function of the window and buffer layer materials and also as a function of various other parameters including the thickness of the buffer layer materials and the minority carrier diffusion length in these materials. The results showed that NiO thin films offer better performances, especially when combined with ZnO or SnO_2 window layers, respectively. The corresponding models with structures $ZnO(n^+)/NiO(n)/CH_3NH_3Sn_{0.75}Ge_{0.25}I_3(p)$ and $SnO_2(n^+)/NiO(n)/CH_3NH_3Sn_{0.75}Ge_{0.25}I_3(p)$ give an internal quantum efficiency of 72.7% and 70.9% respectively.

Keywords

Perovskites, Modeling, Lead-free Perovskite Solar Cell

1. Introduction

In recent years, solar cells based on organic/inorganic hybrid materials with a perovskite structure have developed very rapidly, and their photovoltaic conversion efficiencies have increased from 3.8% in 2009 to 25.2% in 2019 [1, 2]. The high-performance perovskite solar cells currently reported are mainly lead-based materials [3, 4]. The presence of lead, which is very harmful to humans and environment, as well as the stability issue of these materials are major challenges for the development of these photovoltaic structures [17, 18]. In response to these difficulties, a large number of alternative absorber materials based on lead-free or low-lead perovskites and inorganic perovskites have been developed. Theoretically, lead can be replaced by metals such as tin (Sn) [5, 6], bismuth (Bi) [7, 8], copper (Cu) [9], germanium (Ge) [10] or antimony

*Corresponding author: saliou12.seck@ucad.edu.sn (Saliou Seck)

Received: 4 October 2025; **Accepted:** 18 October 2025; **Published:** 31 October 2025

(Sb) [11, 12].

In this work, we carried out a modeling study of photovoltaic devices based on a $CH_3NH_3Sn_{0.75}Ge_{0.25}I_3$-type perovskite material in which the germanium content is varied from 0 to 1.

In thin-film solar cells, window and buffer layers play a decisive role in optimizing photovoltaic performances of devices.

A wide band-gap window layer which allows light to pass through while minimizing reflection losses and helps limit recombination of charge carriers on the surface, is required. The buffer layer, which is an interface layer, is also a wide band-gap layer allowing an adaptation of energy levels by reducing the energy barrier between materials to facilitate the transport of charges carriers. It also limits defects that can trap charges carriers and reduce the performance of the device.

In our recent work, a modeling and analysis of a mixed Sn-Ge lead free perovskite based solar cells have been carried out [17]. This study shows that the best photovoltaic devices are obtained for values of the germanium (Ge) content close to 0.25. In the range 0 to 1 of the Germanium content, the highest internal quantum efficiency (65.8%) is obtained for a value of y = 0.25 and for an absorber thickness of about 0.5 µm.

The thin-film photovoltaic devices investigated in this work are based on $CH_3NH_3Sn_{0.75}Ge_{0.25}I_3$ lead-free perovskite absorber material. Thin films of ZnO, TiO_2 and SnO_2 were chosen as window layers. The buffer layer materials used which are Cu_2O and NiO ensure good electrical contact and the formation of the n-p junction with the absorber $CH_3NH_3Sn_{0.75}Ge_{0.25}I_3$ material. With the above window and buffer layer materials, the following photovoltaic devices $ZnO(n+)/Cu_2O(n)/CH_3NH_3Sn_{0.75}Ge_{0.25}I_3(p)$, $TiO_2(n+)/Cu_2O(n)/CH_3NH_3Sn_{0.75}Ge_{0.25}I_3(p)$, $SnO_2(n+)/Cu_2O(n)/CH_3NH_3Sn_{0.75}Ge_{0.25}I_3(p)$ and $ZnO(n+)/NiO(n)/CH_3NH_3Sn_{0.75}Ge_{0.25}I_3(p)$, $TiO_2(n+)/NiO(n)/CH_3NH_3Sn_{0.75}Ge_{0.25}I_3(p)$, $SnO_2(n+)/NiO(n)/CH_3NH_3Sn_{0.75}Ge_{0.25}I_3(p)$ have been designed. In a recent work, the influence of window layers on the spectral evolution of the total current flowing through such solar cells, have been investigated [18].

In the present work we investigate the influence of physical parameters of buffer layers on the internal quantum efficiency of these photovoltaic cells.

2. Theoretical Approach and Model

The equations used to model solar cell operation are based on the continuity equations of the minority carriers in each part of the solar cell [17, 18]. These continuity equations make it possible to study all the phenomena that occur in semiconductors, and to determine the properties of devices manufactured using these materials.

The space charge region is assumed to lie between the two layers n-type buffer layer Cu_2O or NiO and p-type $CH_3NH_3Sn_{0.75}Ge_{0.25}I_3$. The electric field is also assumed to be zero outside this region. In the steady-state case, the continuity equations are given by:

$$\frac{1}{q}div\overrightarrow{J_n}+G_n-R_n=0$$

$$-\frac{1}{q}div\overrightarrow{J_p}+G_p-R_p=0$$

In the absence of an electric field, we can have:

$$\overrightarrow{J_n}=qD_n.\overrightarrow{grad}(n)$$

$$\overrightarrow{J_p}=-qD_p.\overrightarrow{grad}(p)$$

Our calculations are limited to the one-dimensional case. The solar cell model used in this work is illustrated in Figure 1 [17, 18].

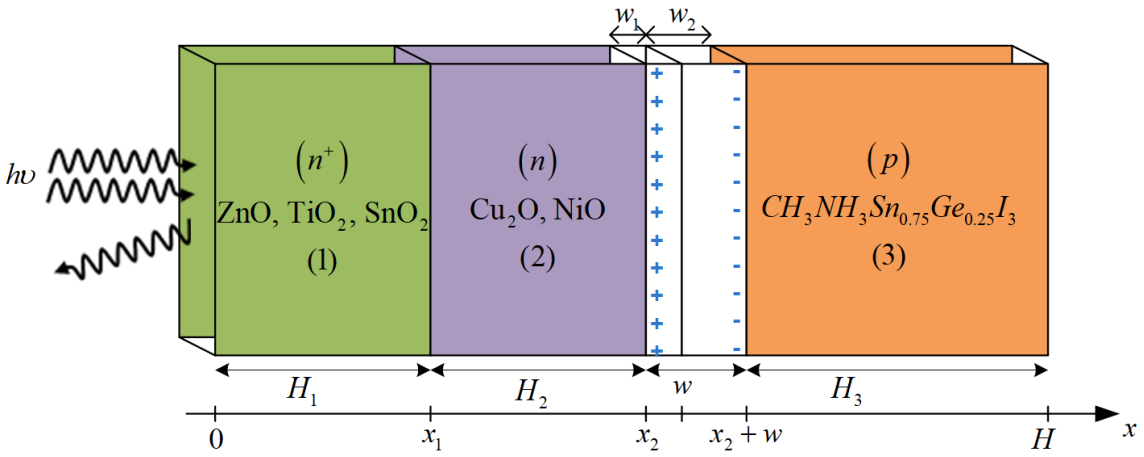

Figure 1. *$CH_3NH_3Sn_{0.75}Ge_{0.25}I_3$(p) perovskite solar cell Model.*

Its structure is (n^+) – Window layer / (n) – Buffer layer / (p) – $CH_3NH_3Sn_{0.75}Ge_{O.25}I_3$. The absorber layer is the $CH_3NH_3Sn_{0.75}Ge_{0.25}I_3$ perovskite. It is a p-type semiconductor material and has a function of absorbing incident photons from solar radiation to generate electron-hole pairs [17, 18]. The particular feature of this material is to have forbidden band width which can be modulated according its germanium content germanium. The forbidden bandwidth is 1.3 eV for $CH_3NH_3SnI_3$ $(y=0)$ and 2.0 eV for $CH_3NH_3GeI_3$ $(y=1)$, which influences the optoelectronic properties of the solar cell. By enhancing the germanium content, we can thus continuously vary the band gap width between 1.3 eV and 2.0 eV and obtain different solar cells [17, 18].

The Cu_2O or NiO buffer layer, of a few nanometers thick, is deposited on the surface of $CH_3NH_3Sn_{0.75}Ge_{0.25}I_3$. This n-type semiconductor layer provides the n-p junction with the absorber and acts as an interface with the window layer [17, 18]. With a direct gap of 2.1 eV, the non-toxic Cu_2O is considered one of the most promising materials for photovoltaic applications. The window layer which a transparent conductive oxide ZnO, TiO_2 or SnO_2, completes the solar cell structure. Its thickness varies from 0.55 µm to 1 µm. The window layer allows incident photons to pass through to the absorber, and also collects charge thanks to its high conductivity.

2.1. Current Density Generated by Light in the Emitter

The current density $J_{ph,E}$ generated by the incident photons in the emitter comprises two contributions: the current density generated in the $(n^+)-Window\ layer$ region, J_{ph_1} and the current density generated in the $(n)-Buffer\ layer$ region, J_{ph_2}.

$$J_{ph,E} = J_{ph_1} + J_{ph_2}$$

2.1.1. Current Density Generated in the (n^+)-Region

In the window layer region (ZnO, TiO_2 or SnO_2) where minority carriers are the holes, the continuity equation is given by:

$$\frac{d^2\Delta_{p_1}}{dx^2} - \frac{\Delta_{p_1}}{{L_{p_1}}^2} = -\frac{g_{WL}}{D_{p_1}}$$

$g_{WL} = \alpha_{WL} F(1-R) e^{-\alpha_{WL} x}$ *and* ${L_{p_1}}^2 = D_{p_1}\tau_{p_1}$ and

$WL \equiv$ Window Layer

In this equation Δ_{p_1} is the minority carries concentration, L_{p_1} and D_{p_1} are the hole diffusion length and the hole diffusion coefficient in the windows layer region, respectively.

τ_{p_1} and α_{WL} represent the hole lifetime and absorption coefficient of the windows layer respectively.

R is the reflection coefficient and $F(E,\lambda)$ is incident photon flux of energy E and wavelength $\lambda(nm)$.

The resolution of this equation was make taking into account the following boundary conditions:

$$D_{p_1}\frac{\partial\Delta_{p_1}}{\partial x} = S_{p_1}\times\Delta_{p_1} \rightarrow \text{ for x = 0}$$
$$\Delta_{p_1} = 0 \rightarrow \text{ for x = } x_1$$

Where S_{p_1} is the recombination velocity on the front surface of the window layer.

The photocurrent J_{ph_1} in this region is given by:

$$J_{ph_1} = -qD_{p_1}\frac{\partial\Delta_{p_1}(x_1)}{\partial x}$$

$$J_{ph_1} = \frac{q\alpha_{WL}F(1-R)L_{p_1}}{\left(\alpha_{WL}{}^2 L_{p_1}{}^2 - 1\right)}\left\{\frac{\left(\frac{S_{p_1}L_{p_1}}{D_{p_1}} + \alpha_{WL}L_{p_1}\right) - e^{-\alpha_{WL}x_1}\left[\frac{S_{p_1}L_{p_1}}{D_{p_1}}ch\left(\frac{x_1}{L_{p_1}}\right) + sh\left(\frac{x_1}{L_{p_1}}\right)\right]}{\frac{S_{p_1}L_{p_1}}{D_{p_1}}sh\left(\frac{x_1}{L_{p_1}}\right) + ch\left(\frac{x_1}{L_{p_1}}\right)} - \alpha_{WL}L_{p_1}e^{-\alpha_{WL}x_1}\right\}$$

2.1.2. Current Density Generated in the n - Region

In this region, which consists of a thin layer of Cu_2O or NiO serving as a buffer layer, the minority carriers are the holes. The continuity equation for the minority carriers is given by:

$$\frac{d^2\Delta_{p_2}}{dx^2} - \frac{\Delta_{p_2}}{{L_{p_2}}^2} = -\frac{g_{BL}}{D_{p_2}}$$

Where:

$g_{BL} = \alpha_{BL}F(1-R)e^{-\alpha_{WL}x_1}.e^{-\alpha_{BL}(x-x_1)}$ and ${L_{p_2}}^2 = D_{p_2}\tau_{p_2}$

Where BL stands for Buffer Layer (Cu_2O, NiO).

Δ_{p_1} is the minority carries concentration. L_{p_2} and D_{p_2} are the hole diffusion length and the hole diffusion coefficient in the buffer layer region, respectively.

τ_{p_2} and α_{BL} represent the hole lifetime and absorption

coefficient of the buffer layer respectively.

Taking into account the following boundary conditions defined as follows,

$$D_{p_2}\frac{\partial \Delta_{p_2}}{\partial x} = S_{p_2}\times\Delta_{p_2} + D_{p_1}\times\frac{\partial \Delta_{p_1}}{\partial x} \rightarrow x = x_1$$

$$\Delta_{p_2} = 0 \rightarrow \text{for } x = x_2$$

the photocurrent in the $x_1 \le x \le x_2$ region is given by:

$$J_{ph_2} = -qD_{p_2}\frac{\partial \Delta_{p_2}(x_2)}{\partial x}$$

$$J_{ph_2} = \frac{q\alpha_{BL}F(1-R)L_{p_2}e^{-\alpha_{WL}x_1}}{\left(\alpha_2{}^2L_{p_2}{}^2-1\right)}\left\{\frac{\left(\frac{S_{p_2}L_{p_2}}{D_{p_2}}+\alpha_{BL}L_{p_2}\right)-e^{-\alpha_{BL}(x_2-x_1)}\left[\frac{S_{p_2}L_{p_2}}{D_{p_2}}ch\left(\frac{x_2-x_1}{L_{p_2}}\right)+sh\left(\frac{x_2-x_1}{L_{p_2}}\right)\right]}{\frac{S_{p_2}L_{p_2}}{D_{p_2}}sh\left(\frac{x_2-x_1}{L_{p_2}}\right)+ch\left(\frac{x_2-x_1}{L_{p_2}}\right)}\right\}+\frac{J_{ph_1(x_1)}}{\frac{S_{p_2}L_{p_2}}{D_{p_2}}sh\left(\frac{x_2-x_1}{L_{p_2}}\right)+ch\left(\frac{x_2-x_1}{L_{p_2}}\right)}$$

$$-\alpha_{BL}L_{p_2}e^{-\alpha_{BL}(x_2-x_1)}$$

2.2. Current Density Generated in Space Charge Area

In the charge space region, carrier recombination may be neglected. Indeed, it is assumed that the transit time of the free carriers in this zone is much shorter than their lowest lifetime because of the strong electric field which prevails therein. So, carriers will not have time to recombine and will all be collected.

In this region, the current density is given by:

$$J_{ZCE} = -qF(1-R)e^{-\alpha_{WL}x_1}e^{-\alpha_{BL}(x_2-x_1)}\left[e^{-\alpha_{BL}w_1}-1\right]-qF(1-R)e^{-\alpha_{WL}x_1}e^{-\alpha_{BL}\left[(x_2+w_1)-x_1\right]}\left[e^{-\alpha_{MASGI}w_2}-1\right]$$

2.3. Current Density Generated in the p – Type Region

In this region, the photo-current is an electron due current. The continuity equation for minority carriers (electrons) is given by:

$$\frac{d^2\Delta_{n_3}}{dx^2}-\frac{\Delta_{n_3}}{L_{n_3}{}^2} = -\frac{g_{MASGI}}{D_{n_3}}$$

Where:

$g_{MASGI} = \alpha_{MASGI}F(1-R)e^{-\alpha_{WL}x_1}.e^{-\alpha_{BL}\left[(x_2+w_1)-x_1\right]}.e^{-\alpha_{MASGI}\left[x-(x_2+w_1)\right]}$ and $L_{n_3}{}^2 = D_{n_3}\tau_{n_3}$

Δ_{n_3} is the minority carries concentration. L_{n_3} and D_{n_3} are the electron diffusion length and the electron diffusion coefficient in the absorber layer region, respectively.

τ_{n_3} represent the electron lifetime and α_{MASGI} the absorption coefficient of the absorber $CH_3NH_3Sn_{0.75}Ge_{0.25}I_3$ layer.

With boundary conditions defined as follows:

$$D_{n_3}\frac{\partial \Delta_{n_3}}{\partial x} = -S_{n_3}\times\Delta_{n_3} \rightarrow \text{for } x = H$$

$$\Delta_{n_3} = 0 \rightarrow \text{for } x = x_2 + w$$

we get the following expression for the photocurrent in the absorber layer:

$$J_{ph_3} = qD_{n_3}\frac{\partial \Delta_{n_3}(x_2+w)}{\partial x}$$

$$= -\frac{q\alpha_{MASGI}F(1-R)L_{n_3}e^{-\alpha_{WL}x_1}e^{-\alpha_{BL}(x_2-x_1+w_1)}}{\left(\alpha_3{}^2L_{n_3}{}^2-1\right)}$$

$$\times\left\{\frac{\left(\alpha_{MASGI}L_{n_3}-\frac{S_{n_3}L_{n_3}}{D_{n_3}}\right)e^{-\alpha_{MASGI}\left[H-(x_2+w_1)\right]}+e^{-\alpha_{MASGI}w_2}\left[\frac{S_{n_3}L_{n_3}}{D_{n_3}}ch\left(\frac{H-(x_2+w)}{L_{n_3}}\right)+sh\left(\frac{H-(x_2+w)}{L_{n_3}}\right)\right]}{\frac{S_{n_3}L_{n_3}}{D_{n_3}}sh\left(\frac{H-(x_2+w)}{L_{n_3}}\right)+ch\left(\frac{H-(x_2+w)}{L_{n_3}}\right)}\right\}$$

2.4. Expression of the Total Photocurrent

The total photocurrent results from the contributions of the different parts of the cell [17, 18]. For a given wavelength, it represents, for our model, the sum of all the above current components, which include the hole diffusion currents in the window and buffer regions, the current generated in the space charge region and the electron diffusion current in the p-type region.

$$J_{ph,T} = J_{ph,E} + J_{ZCE} + J_{ph_3}$$

The internal quantum efficiency is then given:

$$IQE = \frac{J_{ph,T}}{qF(1-R)}$$

After developing our model and establishing the governing equations, we calculated the total current flowing through the solar cell using the absorption coefficients of ZnO and Cu_2O as a function of photon energy. The absorption coefficients values were taken from Zhang [13] et al. and Kar et al. [14]. Those of the perovskite $CH_3NH_3Sn_{0.75}Ge_{0.25}I_3$ materials are given by S. Nagane [15] for photon energies ranging from 1.2eV to 3.0eV. We have approximately completed the values by extrapolation for photons of energy below 1.2eV and for photons of energy above 3.0eV. This makes it possible to cover the entire visible spectrum and achieve higher efficiency.

3. Results and Discussion

3.1. Influence of the Buffer Thickness and Influence of the Diffusion Length of Minority Carriers in Buffer on the Internal Quantum Efficiency

3.1.1. $ZnO(n^+)/Cu_2O(n)/CH_3NH_3Sn_{0.75}Ge_{0.25}I_3(p)$ Structure Model

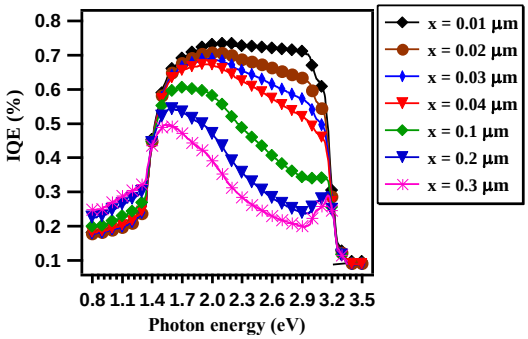

Figure 2. *Influence of the Cu_2O layer thickness on the internal quantum efficiency: case of the solar cell with ZnO window layer.*

Figure 2 shows the evolution of the internal quantum efficiency of the device for different values of the Cu_2O buffer layer thickness. The minority carrier diffusion length in the Cu_2O layer is $0.05\ \mu m$ while its thickness values are varied from $0.01\ \mu m$ to $0.3\ \mu m$. The hole diffusion length and the ZnO window layer thickness are set at $0.55\ \mu m$ and $0.55\ \mu m$, respectively. The electron diffusion length in the $CH_3NH_3Sn_{0.75}Ge_{0.25}I_3$ absorber layer is set at to $0.5\ \mu m$ and its thickness at $0.5\ \mu m$.

Figure 3 shows the effect of the minority carrier diffusion length in the Cu_2O layer on the internal quantum efficiency. The thickness of the Cu_2O layer is set at $0.05\ \mu m$. The diffusion length of the holes varies from $0.01\ \mu m$ to $0.3\ \mu m$.

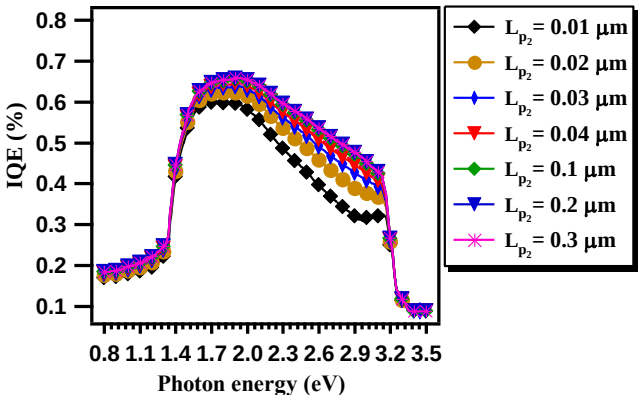

Figure 3. *Evolution of the internal quantum efficiency with the minority carrier diffusion length in the Cu_2O buffer layer: case of the solar cell with the ZnO window layer.*

In Figure 2, the variation in the thickness of the layer shows a drop in internal quantum efficiency for values greater than the carrier diffusion length, and becomes weak for energies greater than 2 eV. Indeed, when the value of the Cu_2O thickness is large compared to the value of the diffusion length, the majority of the carriers photogenerated in this region do not reach the junction to contribute to the current delivered by the solar cell. Instead, they are absorbed by the Cu_2O (in the energy range above 2.1 eV) or recombine. To prevent this from happening, it is important to reduce the value of the thickness relative to the carrier diffusion length in the design to improve the efficiency of the photovoltaic device, as shown in Figure 2.

3.1.2. $TiO_2(n^+)/Cu_2O(n)/CH_3NH_3Sn_{0.75}Ge_{0.25}I_3(p)$ Structure Model

Figure 4 shows the evolution of the internal quantum efficiency for different values of Cu_2O layer thickness. The carrier diffusion length of the Cu_2O layer is $0.05\ \mu m$, and the thickness values range from $0.01\ \mu m$ to $0.3\ \mu m$. The hole diffusion length and thickness of the TiO_2 window layer is

0.55 µm and 0.55 µm respectively. The electron scattering length of the $CH_3NH_3Sn_{0.75}Ge_{0.25}I_3$ absorber layer is estimated at and its thickness at 0.5 µm.

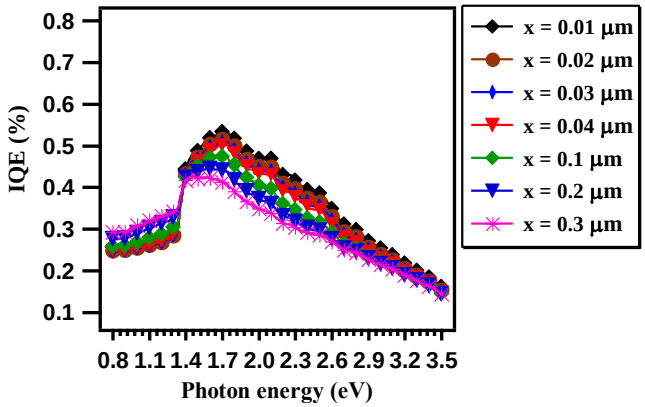

Figure 4. *Influence of the Cu_2O buffer layer thickness on the internal quantum efficiency: case of the solar cell with TiO_2 window layer.*

Figure 5 shows the internal quantum efficiency for different values of minority carrier scattering lengths in the Cu_2O layer. Hole scattering lengths are varied from 0.01 µm to 0.3 µm. The thickness of the Cu_2O layer is fixed at 0.05 µm.

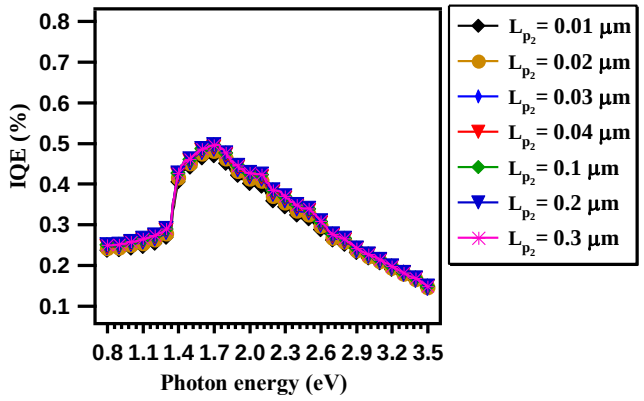

Figure 5. *Evolution of the internal quantum efficiency with the minority carrier diffusion lengths in the Cu_2O buffer layer: case of the solar cell with the TiO_2 window layer.*

The structure $TiO_2(n^+)/Cu_2O(n)/CH_3NH_3Sn_{0.75}Ge_{0.25}I_3(p)$ exhibits lower internal quantum efficiency values as a function of energy than the structure $ZnO(n^+)/Cu_2O(n)/CH_3NH_3Sn_{0.75}Ge_{0.25}I_3(p)$. For thickness values between 0.01 µm and 0.04 µm, the internal quantum efficiency is between 50% and 60%. For thicknesses in the range, the overall internal quantum efficiency remains low for values between 40% and 50%. These low internal quantum efficiency values can be explained by the fact that when the layer thickness is large relative to the diffusion length, the majority of photogenerated carriers in this region do not reach the junction to contribute to the current delivered by the solar cell. These are absorbed by the (in the energy range above 2.1 eV) or recombine.

3.1.3. $SnO_2(n^+)/Cu_2O(n)/CH_3NH_3Sn_{0.75}Ge_{0.25}I_3(p)$ Structure Model

The evolution of the internal quantum efficiency for different values of Cu_2O layer thickness in the $SnO_2(n^+)/Cu_2O(n)/CH_3NH_3Sn_{0.75}Ge_{0.25}I_3(p)$ structure shown in the figure. Cu_2O thickness values range from 0.01 µm and 0.3 µm. The hole diffusion length and thickness of the ZnO window layer is 0.55 µm et 0.55 µm respectively. The electron scattering length of the $CH_3NH_3Sn_{0.75}Ge_{0.25}I_3$ absorber layer is estimated at 0.5 µm and its thickness at 0.5 µm.

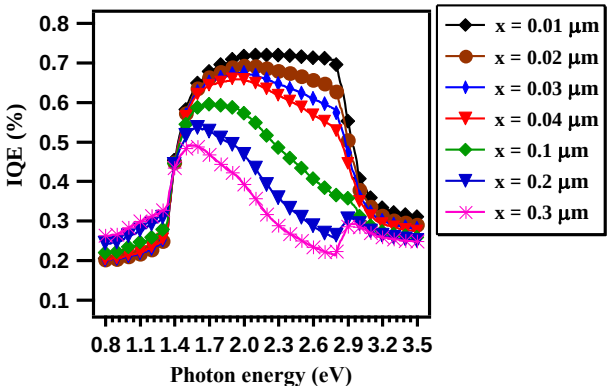

Figure 6. *Influence of the Cu_2O buffer layer thickness on the internal quantum efficiency: case of the solar cell with ZnO window layer.*

The effect of the Cu_2O layer's minority carrier diffusion length on the internal quantum efficiency is shown in figure 7. The thickness of the Cu_2O layer is fixed at 0.05 µm. The diffusion lengths of the holes vary from 0.01 µm to 0.3 µm.

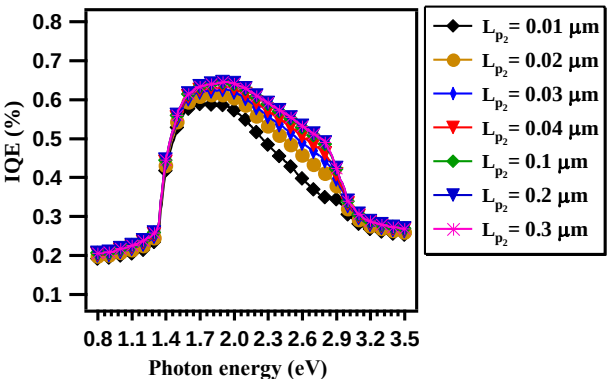

Figure 7. *Evolution of the internal quantum efficiency with the minority carrier diffusion lengths in the Cu_2O buffer layer: case of the solar cell with the SnO_2 window layer.*

Varying the thickness of the Cu_2O window layer in the case of the structural model shows a good improvement in the internal quantum efficiency of the total current flowing through the solar cell. For small thickness values between $0.01\ \mu m$ and $0.04\ \mu m$, the internal quantum efficiency is between 60% and 80%. Those in the $0.1\ \mu m - 0.3\ \mu m$ range give the best performance. Internal quantum efficiency drops from 70.2% to 64.3% for thicknesses between $0.1\ \mu m$ and $0.3\ \mu m$. This is because, for each given thickness, there is a diffusion length at which the internal quantum efficiency is maximum.

3.2. Influence of the Thickness and Minority Carrier Diffusion Length on the NiO Buffer Layer on the Internal Quantum Efficiency

In this section, we have also used NiO as buffer layer. NiO has a gap energy of $3.4\ eV$. The NiO buffer layer, also acts as a window, enabling the electrical transition between the and the absorber material $CH_3NH_3Sn_{0.75}Ge_{0.25}I_3$. The absorption coefficients values of the NiO layer were taken from [16] for photon energies ranging from $1.2\ eV$ to $3.5\ eV$.

With the aim of optimizing the internal quantum efficiency obtained with the Cu_2O material and selecting the best performing structure, in this section we study the influence of the layer with the different window layers ZnO, TiO_2 and SnO_2. The same continuity equations established and solved in Section 2 were used for the different models with the NiO material as buffer layer.

3.2.1. $ZnO(n^+)/NiO(n)/CH_3NH_3Sn_{0.75}Ge_{0.25}I_3(p)$ Structure Model

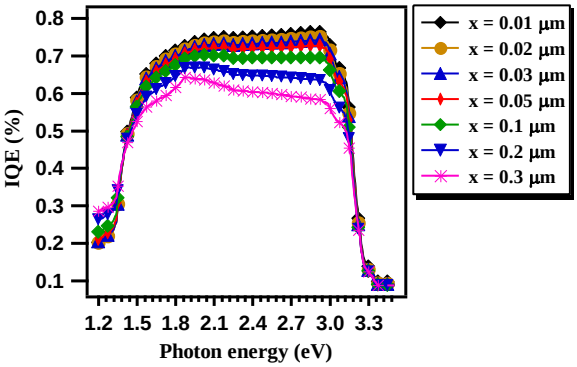

Figure 8. *Influence of the NiO buffer layer thickness on the internal quantum efficiency: case of the solar cell with ZnO window layer.*

Figure 8 shows the influence of layer thickness on internal quantum efficiency. The diffusion length of NiO carriers is fixed at $0.05\ \mu m$. We vary the thickness from $0.01\ \mu m$ to $0.3\ \mu m$. The carrier scattering length in the ZnO layer and its thickness are evaluated at 0.55 micrometers. For the perovskite layer, its thickness is set at $0.55\ \mu m$ and the diffusion length of its carriers at $0.55\ \mu m$.

Figure 9 shows the internal quantum efficiency as a function of energy for different values of carrier scattering lengths in the NiO layer. Its thickness is fixed at $0.05\ \mu m$. The diffusion length varies from $0.01\ \mu m$ to $0.3\ \mu m$. The carrier diffusion length in the *ZnO* layer and its thickness are evaluated at $0.55\ \mu m$. For the perovskite layer, its thickness is set at $0.5\ \mu m$ and the diffusion length of its carriers at $0.5\ \mu m$.

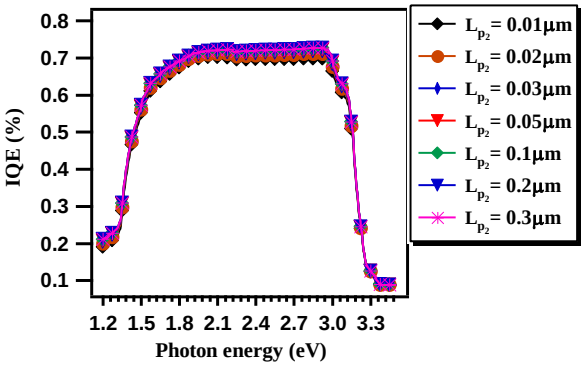

Figure 9. *Evolution of the internal quantum efficiency with the minority carrier diffusion lengths in the NiO buffer layer: case of the solar cell with the ZnO window layer.*

As the thickness of the NiO window layer varies, we see a good improvement in the internal quantum efficiency of the total current flowing through the solar cell. For thicknesses between $0.01\ \mu m$ et $0.1\ \mu m$, the internal quantum efficiency is between 70% and 80%. Those in the $0.01\ \mu m - 0.03\ \mu m$ range give the best performance. Internal quantum efficiency drops from 70.2% to 64.3% for thicknesses between $0.01\ \mu m$ and $0.3\ \mu m$. This is because, for each given thickness, there is a scattering length at which the internal quantum efficiency is maximum.

3.2.2. $TiO_2(n^+)/NiO(n)/CH_3NH_3Sn_{0.75}Ge_{0.25}I_3(p)$ Structure Model

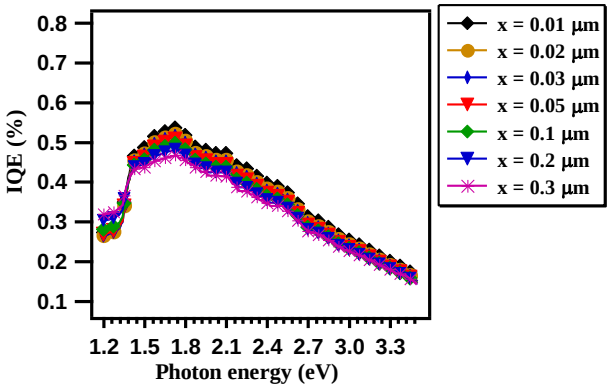

Figure 10. *Influence of the NiO buffer layer thickness on the internal quantum efficiency: case of the solar cell with TiO_2 window layer.*

Figure 10 shows the internal quantum efficiency as a function of energy for different values of NiO layer thickness. The diffusion length of the de carriers is fixed at $0.05\ \mu m$. We vary the thickness from $0.01\ \mu m$ to $0.3\ \mu m$. The carrier diffusion length in the ZnO layer and its thickness are evaluated at $0.55\ \mu m$. For the perovskite layer, its thickness is set at $0.5\ \mu m$ and the diffusion length of its carriers at $0.5\ \mu m$.

Figure 11 shows the evolution of the internal quantum efficiency as a function of energy for different values of diffusion length of the NiO layer of the $TiO_2(n^+)/NiO(n)/CH_3NH_3Sn_{0.75}Ge_{0.25}I_3(p)$ structure model. The thickness of the NiO layer is fixed at $0.05\ \mu m$, and the diffusion length varies from 0.01 to 0.3 mm. The diffusion length of the carriers in the ZnO layer and its thickness are evaluated at 0.55 mm. For the perovskite layer, its thickness is set at 0.5 mm and the diffusion length of its carriers at 0.5 mm.

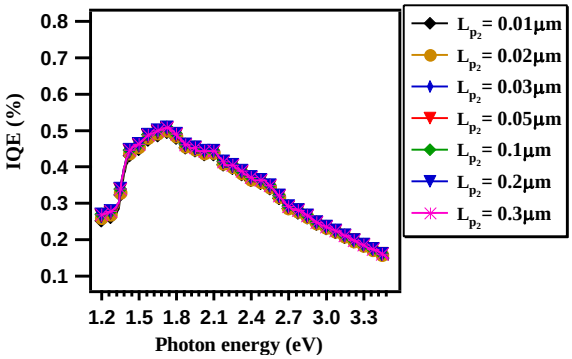

Figure 11. *Evolution of the internal quantum efficiency with the minority carrier diffusion lengths in the NiO buffer layer: case of the solar cell with the TiO_2 window layer.*

3.2.3. $SnO_2(n^+)/NiO(n)/CH_3NH_3Sn_{0.75}Ge_{0.25}I_3(p)$ Structure Model

Figure 12 shows the internal quantum efficiency as a function of energy for different values of NiO layer thickness. The scattering length is fixed at $0.05\ \mu m$ and the thickness varies from $0.01\ \mu m$ to $0.3\ \mu m$.

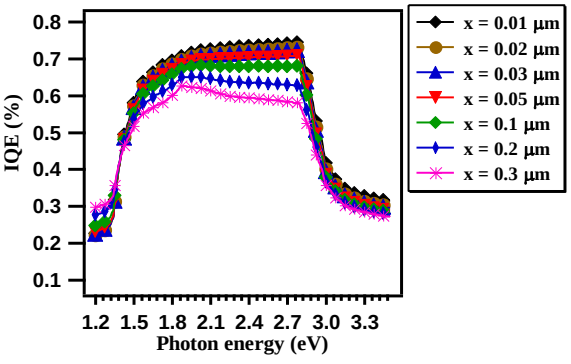

Figure 12. *Influence of the NiO buffer layer thickness on the internal quantum efficiency: case of the solar cell with SnO_2 window layer.*

Figure 13 shows the evolution of the internal quantum efficiency of the $SnO_2(n^+)/NiO(n)/CH_3NH_3Sn_{0.75}Ge_{0.25}I_3(p)$ structure model for different values of the diffusion length of the NiO layer [17, 18]. The thickness is fixed at $0.05\ \mu m$ and the diffusion length varies from $0.01\ \mu m$ to $0.03\ \mu m$. The thickness and diffusion length of the SnO_2 carriers are estimated at $0.55\ \mu m$. The perovskite layer thickness is set at $0.5\ \mu m$ and the carrier diffusion length at $0.5\ \mu m$.

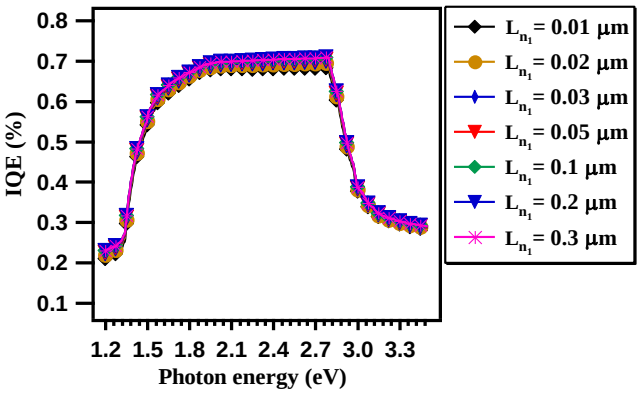

Figure 13. *Evolution of the internal quantum efficiency with the minority carrier diffusion lengths in the NiO buffer layer: case of the solar cell with the SnO_2 window layer.*

As the thickness of the NiO window layer varies, we see a good improvement in the internal quantum efficiency of the total current flowing through the solar cell. For thicknesses between $0.01\ \mu m$ and $0.1\ \mu m$, the internal quantum efficiency is between 70% and 80%. Those in the $0.01\ \mu m$ - $0.03\ \mu m$ range give the best performance. Internal quantum efficiency drops from 68.1% to 62.7% for thicknesses between $0.1\ \mu m$ and $0.3\ \mu m$. This is because, for each given thickness, there is a scattering length at which the internal quantum efficiency is at its maximum.

3.3. Comparative Study of Internal Quantum Efficiency Models with NiO

Figure 14 shows the internal quantum efficiency of the three models studied with different window layers $ZnO(n^+)/NiO(n)/CH_3NH_3Sn_{0.75}Ge_{0.25}I_3(p)$, $TiO_2(n^+)/NiO(n)/CH_3NH_3Sn_{0.75}Ge_{0.25}I_3(p)$ et $SnO_2(n^+)/NiO(n)/CH_3NH_3Sn_{0.75}Ge_{0.25}I_3(p)$. This figure shows the best internal quantum efficiency of the three models. For all three curves, we set the thickness of the ZnO, TiO_2 et SnO_2 (window layers at $0.55\ \mu m$, and the carrier scattering lengths at $0.55\ \mu m$. The values for carrier scattering lengths and NiO layer thicknesses are $0.5\ \mu m$ and $0.05\ \mu m$ respectively. For the $CH_3NH_3Sn_{0.75}Ge_{0.25}I_3$ absorber layer, the carrier diffusion length is equal to $0.5\ \mu m$ and the thickness $0.5\ \mu m$. For the three different models

$ZnO(n^+)/NiO(n)/CH_3NH_3Sn_{0.75}Ge_{0.25}I_3(p)$, $TiO_2(n^+)/NiO(n)/CH_3NH_3Sn_{0.75}Ge_{0.25}I_3(p)$ and $SnO_2(n^+)/NiO(n)/CH_3NH_3Sn_{0.75}Ge_{0.25}I_3(p)$ and the internal quantum efficiency are 72.7%, 50.9% and 70.9% respectively. The ZnO and NiO materials for transport layers with the structure $ZnO(n^+)/NiO(n)/CH_3NH_3Sn_{0.75}Ge_{0.25}I_3(p)$ model give the best internal quantum efficiency of 72.7%.

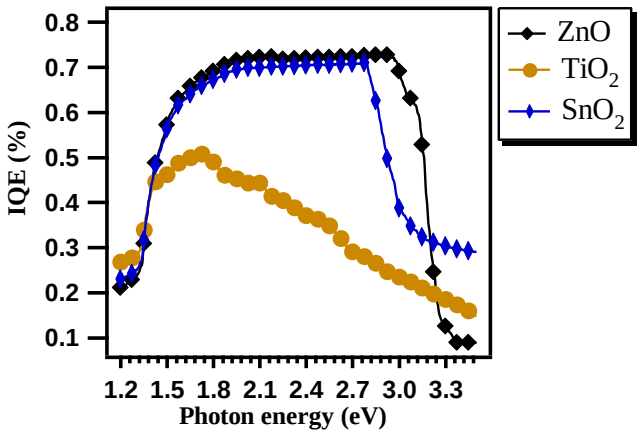

Figure 14. *Internal quantum efficiency as a function of photon energy for the three models: $ZnO(n^+)/NiO(n)/CH_3NH_3Sn_{0.75}Ge_{0.25}I_3(p)$, $TiO_2(n^+)/NiO(n)/CH_3NH_3Sn_{0.75}Ge_{0.25}I_3(p)$ and $SnO_2(n^+)/NiO(n)/CH_3NH_3Sn_{0.75}Ge_{0.25}I_3(p)$.*

4. Conclusion

In this article, we have carried out a theoretical study to determine the internal quantum efficiency of photovoltaic devices using the lead-free perovskite material $CH_3NH_3Sn_{0.75}Ge_{0.25}I_3$ as absorber. The effect of the minority carrier diffusion length and the thickness of the Cu_2O and NiO buffer layers on the spectral evolution of the total current flowing through the solar cell was investigated. The materials ZnO, TiO_2 and SnO_2 were used as transport window layers. This enabled us to obtain the following different structural $ZnO(n^+)/Cu_2O(n)/CH_3NH_3Sn_{0.75}Ge_{0.25}I_3(p)$, $TiO_2(n^+)/Cu_2O(n)/CH_3NH_3Sn_{0.75}Ge_{0.25}I_3(p)$, $SnO_2(n^+)/Cu_2O(n)/CH_3NH_3Sn_{0.75}Ge_{0.25}I_3(p)$ and $ZnO(n^+)/NiO(n)/CH_3NH_3Sn_{0.75}Ge_{0.25}I_3(p)$, $TiO_2(n^+)/NiO(n)/CH_3NH_3Sn_{0.75}Ge_{0.25}I_3(p)$, $SnO_2(n^+)/NiO(n)/CH_3NH_3Sn_{0.75}Ge_{0.25}I_3(p)$ models. Optimization of these structures shows that the best internal quantum efficiency is obtained with the transport window layer materials ZnO and NiO. The corresponding model with structure $ZnO(n^+)/NiO(n)/CH_3NH_3Sn_{0.75}Ge_{0.25}I_3(p)$ gives an internal quantum efficiency of 72.7%.

Abbreviations

IQE	Internal Quantum Efficiency
Ge	Germanium
Sn	Tin
WL	Windows Layer
BL	Buffer Layer

Acknowledgments

This section serves to recognize contributions that do not meet authorship criteria, including technical assistance, donations, or organizational aid. Individuals or organizations should be acknowledged with their full names. The acknowledgments should be placed after the conclusion and before the references section in the manuscript.

Author Contributions

Saliou Seck: Conceptualization, Data curation, Formal Analysis, Methodology, Software, Validation, Writing – original draft, Writing – review & editing

Alioune Sow: Visualization

Mamadou Salif Mane: Visualization

Cheikh Sene: Supervision, Validation, Visualization, Writing – review & editing

Conflicts of Interest

The authors declare no conflicts of interest.

References

[1] A. Kojima, K. Teshima, Y. Shirai, T. Miyasaka, Organometal halide perovskites as visible-light sensitizers for photovoltaic cells J. Am. Chem. Soc. 131 (2009) 6050. https://doi.org/10.1021/ja809598r

[2] Y. C. Zhao, W. K. Zhou, X. Zhou, K. H. Liu, D. P. Yu, Q. Zhao, Quantification of light-enhanced ionic transport in lead iodide perovskite thin films and its solar cell applications Light: Sci. Appl., 6 (2017) 6243. https://doi.org/10.1038/lsa.2016.243

[3] W. J. Yin, T. Shi, Y. Yan, Unique properties of halide perovskites as possible origins of the superior solar cell performance, Adv. Mater., 26 (2014) 4653. https://doi.org/10.1002/adma.201306281

[4] J. Jiang, Q. Wang, Z. Jin, X. Zhang, J. Lei, H. Bin, Z. G. Zhang, Y. Li, S. Liu, Polymer doping for high-efficiency perovskite solar cells with improved moisture stability, Adv. Energy Mater. 8 (2018) 1701757. https://doi.org/10.1002/aenm.201701757

[5] M. H. Kumar, S. Dharani, W. L. Leong, P. P. Boix, R. R. Prabhakar, T. Baikie, C. Shi, H. Ding, R. Ramesh, M. Asta, M. Graetzel, S. G. Mhaisalkar, N. Mathews, Lead‐free halide perovskite solar cells with high photocurrents realized through vacancy modulation, Adv. Mater., 26 (2014) 7122. https://doi.org/10.1002/adma.201401991

[6] D. H. Cao, C. C. Stoumpos, T. Yokoyama, J. L. Logsdon, T. B. Song, O. K. Farha, M. R. Wasielewski, J. T. Hupp, M. G. Kanatzidis, Thin Films and Solar Cells Based on Semiconducting Two-Dimensional Ruddlesden–Popper (CH3(CH2)3NH3)2(CH3NH3)n−1SnnI3n+1 Perovskites, ACS Energy Lett., 2 (2017) 982. https://doi.org/10.1021/acsenergylett.7b00202

[7] B. W. Park, B. Philippe, X. Zhang, H. Rensmo, G. Boschloo, E. M. J. Johansson, Bismuth Based Hybrid Perovskites A3Bi2I9 (A: Methylammonium or Cesium) for Solar Cell Application, Adv. Mater., 27 (2015) 6806. https://doi.org/10.1002/adma.201501978

[8] K. Eckhardt, V. Bon, J. Getzschmann, J. Grothe, F. M. Wisser, S. Kaskel, Crystallographic insights into (CH3NH3)3(Bi2I9): a new lead-free hybrid organic–inorganic material as a potential absorber for photovoltaics, Chem. Commun., 52 (2016) 3058. https://doi.org/10.1039/C5CC10455F

[9] M. Jahandar, J. H. Heo, C. E. Song, K.-J. Kong, W. S. Shin, J. C. Lee, S. H. Im, S. J. Moon, Highly efficient metal halide substituted CH3NH3I(PbI2)1−X(CuBr2)X planar perovskite solar cells, Nano Energy 27 (2016) 330. https://doi.org/10.1016/j.nanoen.2016.07.022

[10] T. Krishnamoorthy, H. Ding, C. Yan, W. L. Leong, T. Baikie, Z. Zhang, M. Sherburne, S. Li, M. Asta, N. Mathews, S. G. Mhaisalkar, Lead-free germanium iodide perovskite materials for photovoltaic application, J. Mater. Chem. 3 (2015) 23829. https://doi.org/10.1039/C5TA05741H

[11] K. M. Boopathi, P. Karuppuswamy, A. Singh, C. Hanmandlu, L. Lin, S. A. Abbas, C. C. Chang, P. C. Wang, G. Li, C. W. Chu, Solution-processable antimony-based light-absorbing materials beyond lead halide perovskites, J. Mater. Chem., 5 (2017) 20843. https://doi.org/10.1039/C7TA06679A

[12] C. Zuo, L. Ding, Angew. Lead-free Perovskite Materials (NH4)3Sb2IxBr9−x, Chem., 56 (2017) 6528. https://doi.org/10.1002/ange.201702265

[13] L. Zhang, W. Liang, How the structures and properties of two-dimensional layered perovskites MAPbI3 and CsPbI3 vary with the number of layers, J. Phys. Chem. Lett., 8 (2017) 1517-1523. https://doi.org/10.1021/acs.jpclett.6b03005

[14] M. Kar, R. Sarkar, S. Pal, P. Sarkar, Lead Free Two-Dimensional Mixed Tin and Germanium Halide Perovskites for Photovoltaic Applications, J. Phys. Chem., 125 (2021) 74−81. https://doi.org/10.1021/acs.jpcc.0c08164

[15] S. Nagane, D. Ghosh, R. L. Z. Hoye, B. Zhao, S. Ahmad, A. B. Walker, M. S. Islam, S. Ogale, A. Sadhanala, Lead-free perovskite semiconductors based on germanium-tin solid solutions: Structural and optoelectronic properties, J. Phys. Chem. C, 122 (2018) 5940−5947. https://doi.org/10.1021/acs.jpcc.8b00480

[16] N. F. A. Shammary, Optical characteristics of NiO thin film on glass formed by chemical spray pyrolysis. Journal of kufa-Physics, 2 (2010).

[17] S. Seck, A. Sow, M. S. Mané, A. Ndiaye, E. M. Keita, B. Ndiaye, B. Mbow, and C. Sène, Modeling and Analysis of a Mixed Sn-Ge Lead Free Perovskite Based Solar Cells, American Journal of Energy Research, (12) 1 (2024) 1-7. https://doi.org/10.12691/ajer-12-1-1

[18] S. Seck, A. Sow, M. S. Mane, M. Faye, E. H. M. Keita, A. Ndiaye, B. Ndiaye, B. Mbow, C. Sene, Influence of Window Layers on the Spectral Evolution of the Total Current Flowing Through a Solar Cell Based on Lead-Free Perovskite Materials, International Journal of Materials Science and Applications, (3) 14 (2025) 79-88. https://doi.org/10.11648/j.ijmsa.20251403.14